Supporting Information

Promoting osmotic energy conversion through fluorinated nanochannel membranes with large-scale exfoliation and low transmission resistance

Zhengmao Ding [1,2], Tiancheng Gu [2], Shouyi Sun [1], Gang Tang [2], Hanli Zhang [1], Teng Wang [2], Yunjun Luo [2,*], Jinjin Li [1,*]

[1] *State Key Laboratory of Tribology in Advanced Equipment, Tsinghua University, Beijing 100084, PR China.*

[2] *Key Laboratory of High Energy Density Materials, Ministry of Education, Beijing Institute of Technology, Beijing 100081, PR China.*

** Corresponding author.*

** Correspondence and requests for materials should be addressed to J. Li (email: lijinjin@mail.tsinghua.edu.cn)*

Supporting Note 1. Potential Calibration

The osmotic energy conversion performance of the Na-MTM composite membranes is evaluated in an H-type electrochemical cell by scanning the *I-V* curves with a KCl concentration gradient across the composite membrane. The equivalent circuit of the system is shown in Figure S10. V_{OC}, E_{redox}, V_{OS}, and $R_{membrane}$ represent the measured open-circuit voltage, the redox potential resulting from the unequal potential drop at the electrode-solution interface, the osmotic potential contributed by the ion-selective membrane, and the internal resistance of the membrane, respectively. The measured V_{OC} actually are composed of E_{redox} and V_{OS} [1]. Therefore, it can be obtained the following equation:

$$V_{OS} = V_{OC} - E_{redox}$$

In this work, the Na-MTM composite membranes were mounted in the electrochemical cell with both sides of the membrane in contact with the salt solution. The testing membrane area was the same as in the previous report [2], approximately 0.03 mm^2. The value of E_{redox} was also measured using the above method except that there is no membrane in the electrochemical cell. Table S2 shows the corresponding values of V_{OC}, E_{redox}, and V_{OS}.

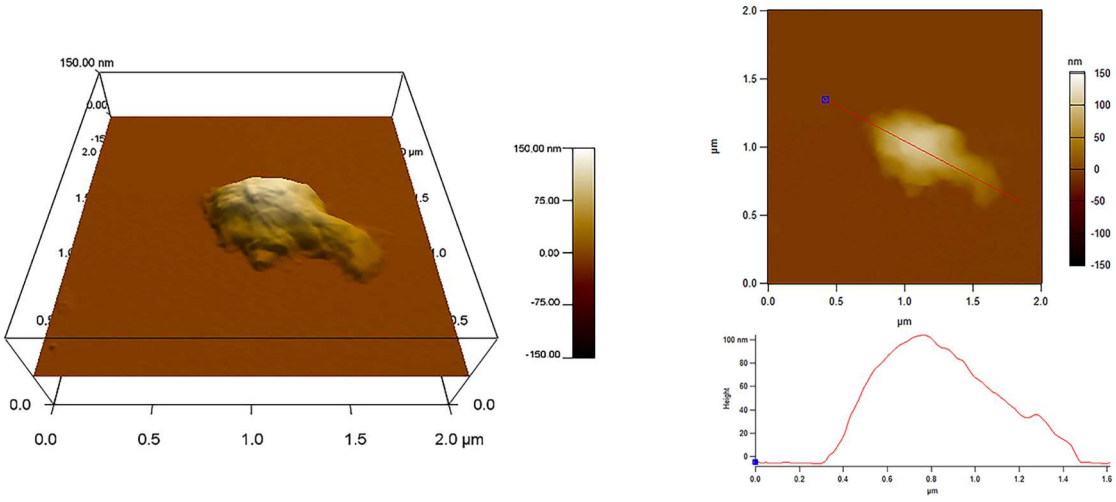

Figure S1. AFM image and height profile of Na-MTM powders. Scale bar, 2.0 µm; z scale, −150.0 to 150.0 nm.

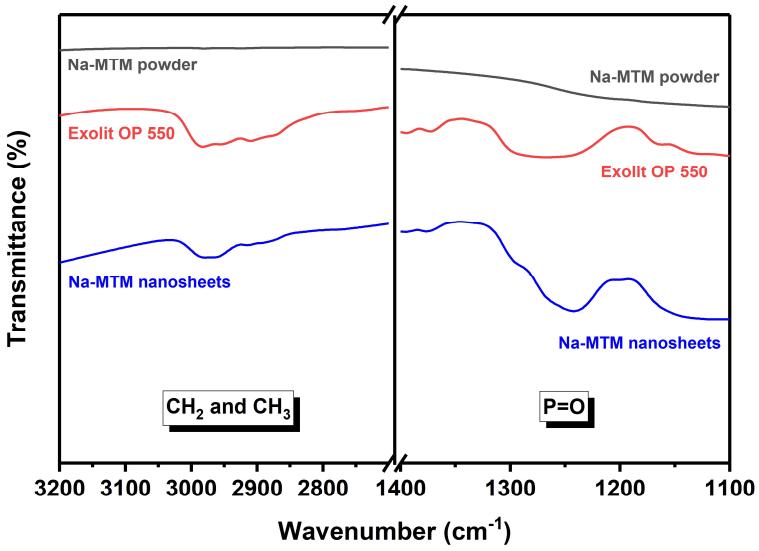

Figure S2. FTIR spectra of Na-MTM powders, Exolit OP 550, and Na-MTM/Exolit OP 550 composite membranes at CH_2, CH_3, and P=O. The peaks of CH_2, CH_3, and P=O from Exolit OP 550 newly detected on the Na-MTM/Exolit OP 550 composite membrane confirms that Exolit OP 550 was attached to the surface of Na-MTM nanosheets.

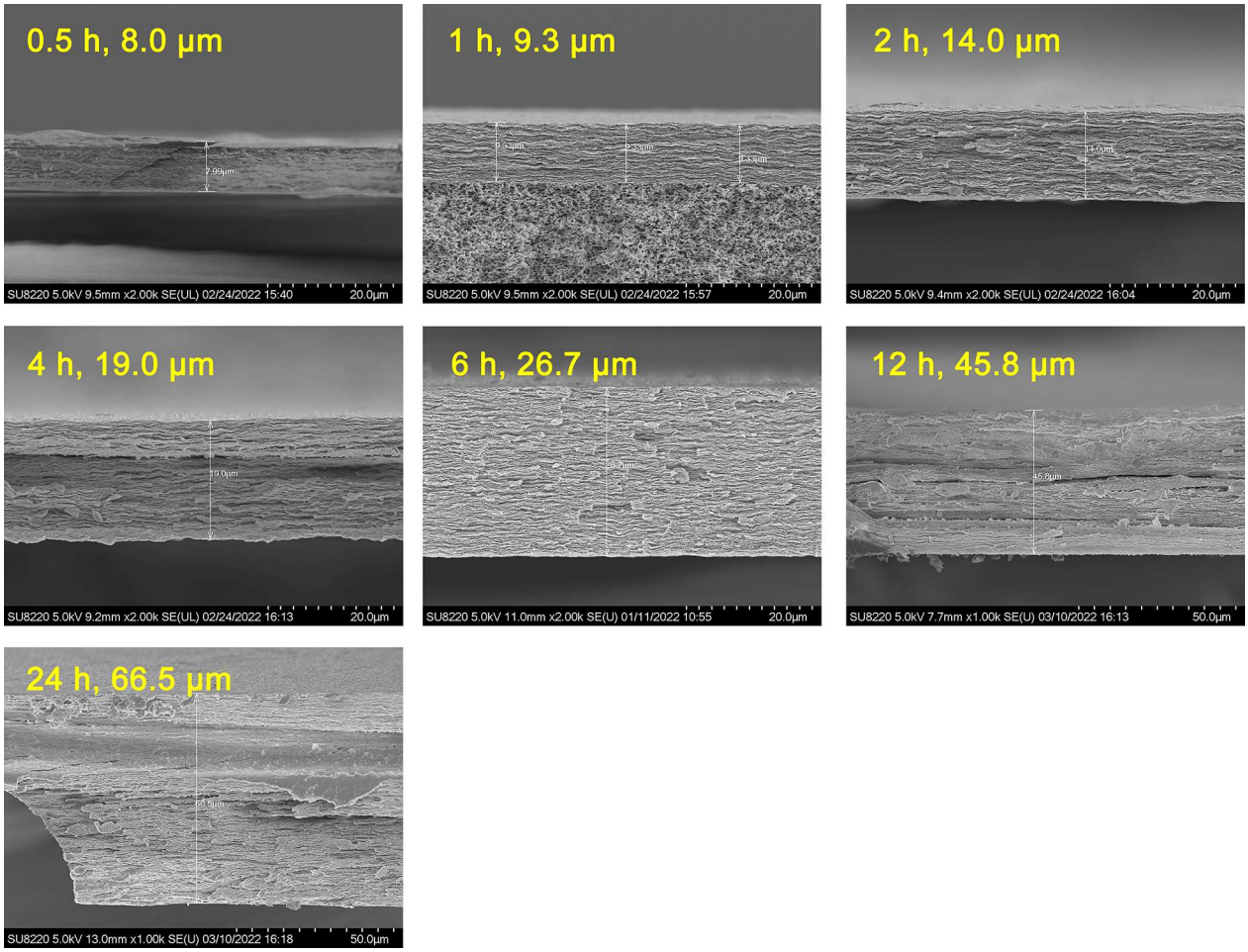

Figure S3. SEM cross-sectional images of the Na-MTM composite membranes with different thicknesses prepared by adjusting the filtration time.

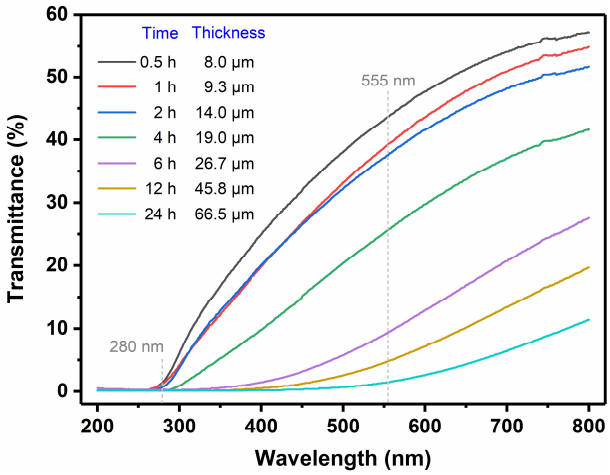

Figure S4. UV-visible transmittances of Na-MTM composite membranes with different thicknesses prepared by adjusting the filtration time.

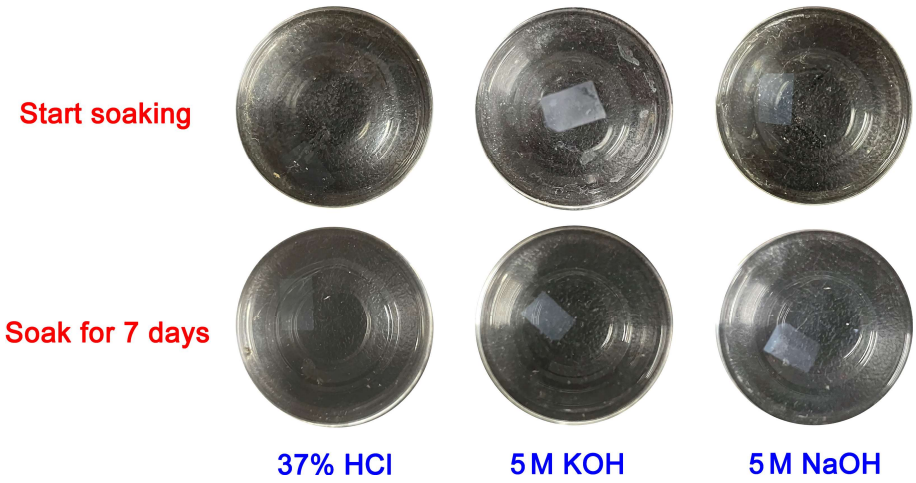

Figure S5. Appearance of the Na-MTM composite membrane immersed in HCl (37%), KOH (5M), and NaOH (5M) solutions.

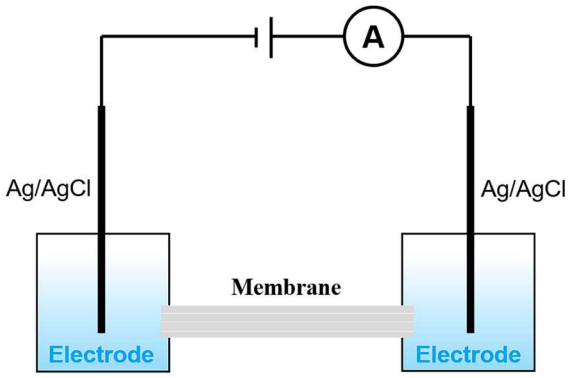

Figure S6. Schematic of the homemade nanofluid device for ion transport in Na-MTM/Exolit OP 550 composite membranes. The cropped rectangular strip of the membrane was encapsulated in the grooved polydimethylsiloxane elastomer. Both sides of the membrane need to be trimmed before testing to ensure that all nanochannels are open.

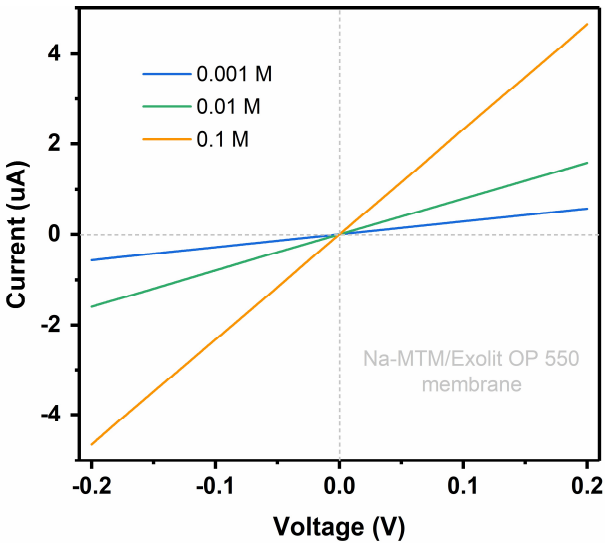

Figure S7. *I–V* curves of Na-MTM/Exolit OP 550 composite membranes after 4 times of washing recorded in neutral KCl electrolyte with different concentrations.

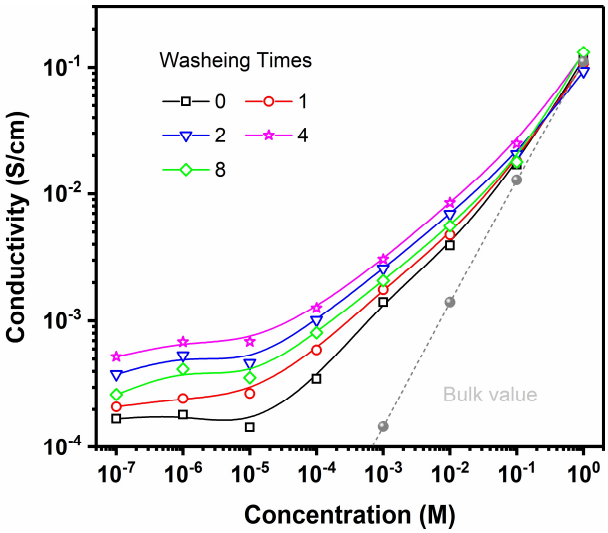

Figure S8. Conductivity measurement of Na-MTM/Exolit OP 550 composite membranes with different washing times as a function of KCl concentration declines non-linearly with the bulk value, indicating a charge-governed ion transport. For the sake of clarity, the corresponding error bars were not added to the data points.

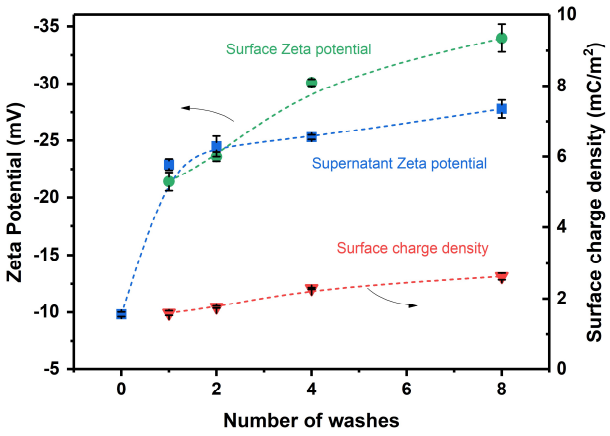

Figure S9. Supernatant ζ, surface ζ, and σ of the Na-MTM/Exolit OP 550 composite membranes with different washing times.

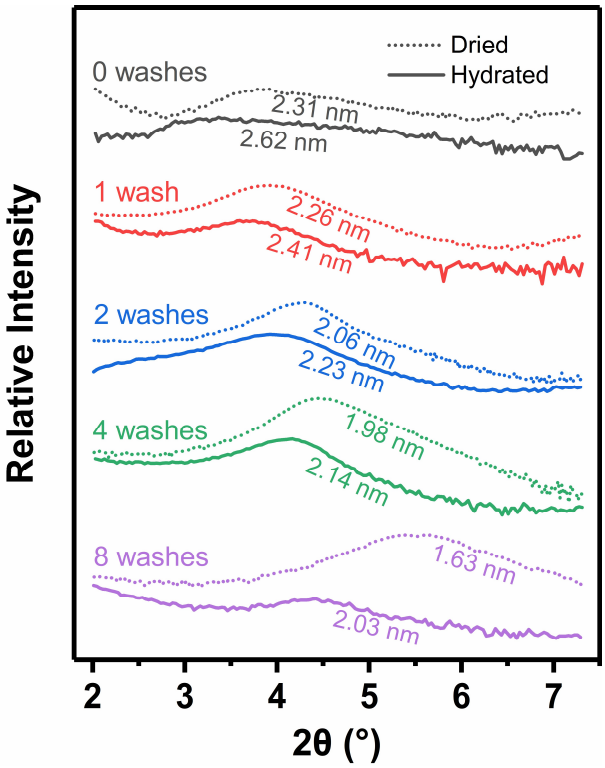

Figure S10. Small-angle XRD patterns show the (001) peak shift of Na-MTM/Exolit OP 550 composite membrane before and after complete hydration with different washing times. The interlayer spacing can be calculated according to Bragg equation. The nanochannel size can be obtained by subtracting the theoretical thickness (~1 nm) of monolayer MTM from the calculated interlayer spacing.

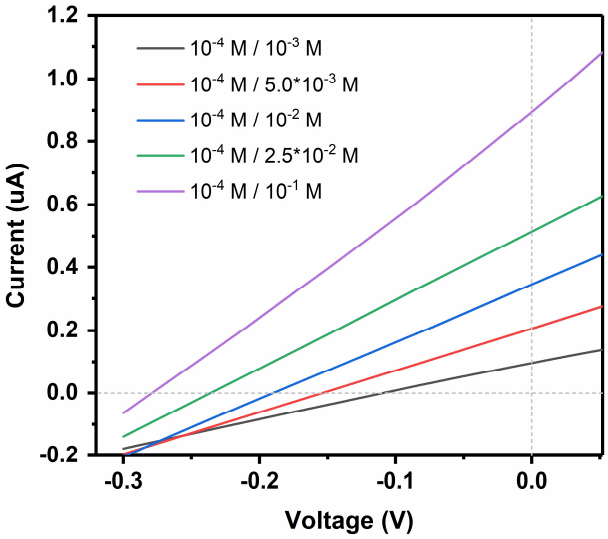

Figure S11. *I–V* curves of the Na-MTM/Exolit OP 550/STFA composite membranes recorded in different KCl concentration gradients. The relevant values obtained from the *I–V* curves are listed in Table S2.

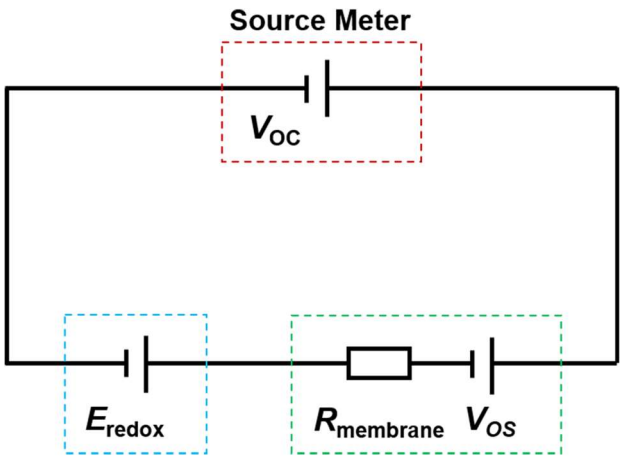

Figure S12. Equivalent circuit diagram of the membrane-based power source.

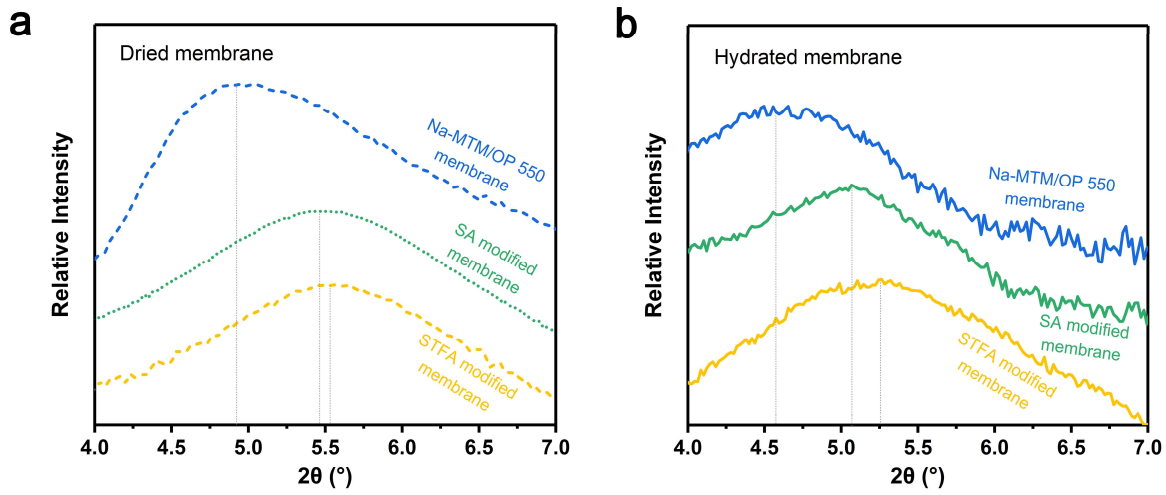

Figure S13. Small-angle XRD patterns show the locally enlarged (001) peak shift for different Na-MTM composite membranes (a) before and (b) after complete hydration.

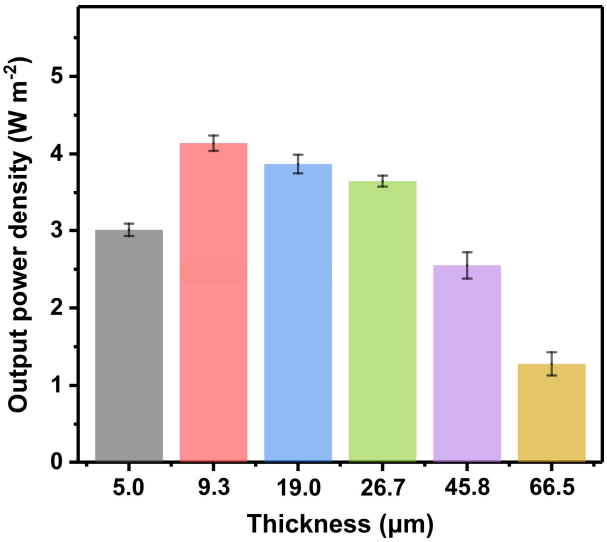

Figure S14. Maximum output power density of the Na-MTM/Exolit OP 550/STFA composite membranes with different washing thicknesses in 0.5 M NaCl/0.01 M NaCl. Thicker membranes increase the resistance to ion transport, but at the same time increase the ion selectivity. Therefore, the change of the maximum output power with the thickness results from the joint action of the two factors. The prepared 9.3 μm membrane has the maximum value.

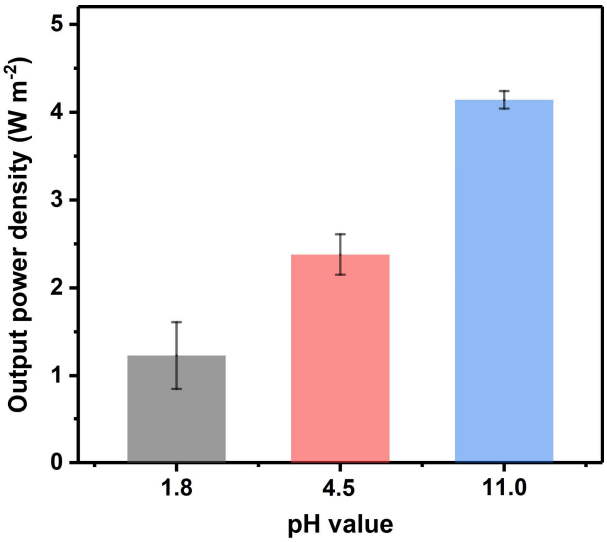

Figure S15. Maximum output power density of the Na-MTM/Exolit OP 550/STFA composite membrane with different solution pH values in 0.5 M NaCl/0.01 M NaCl.

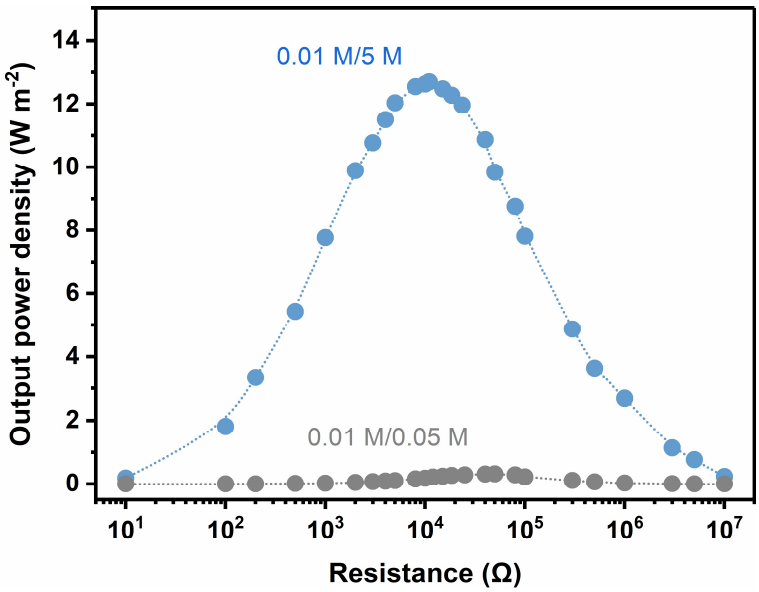

Figure S16. Output power density of Na-MTM/Exolit OP 550/STFA composite membrane depend on the external load resistance in 0.05 M NaCl/0.01 M NaCl and 5 M NaCl/0.01 M NaCl.

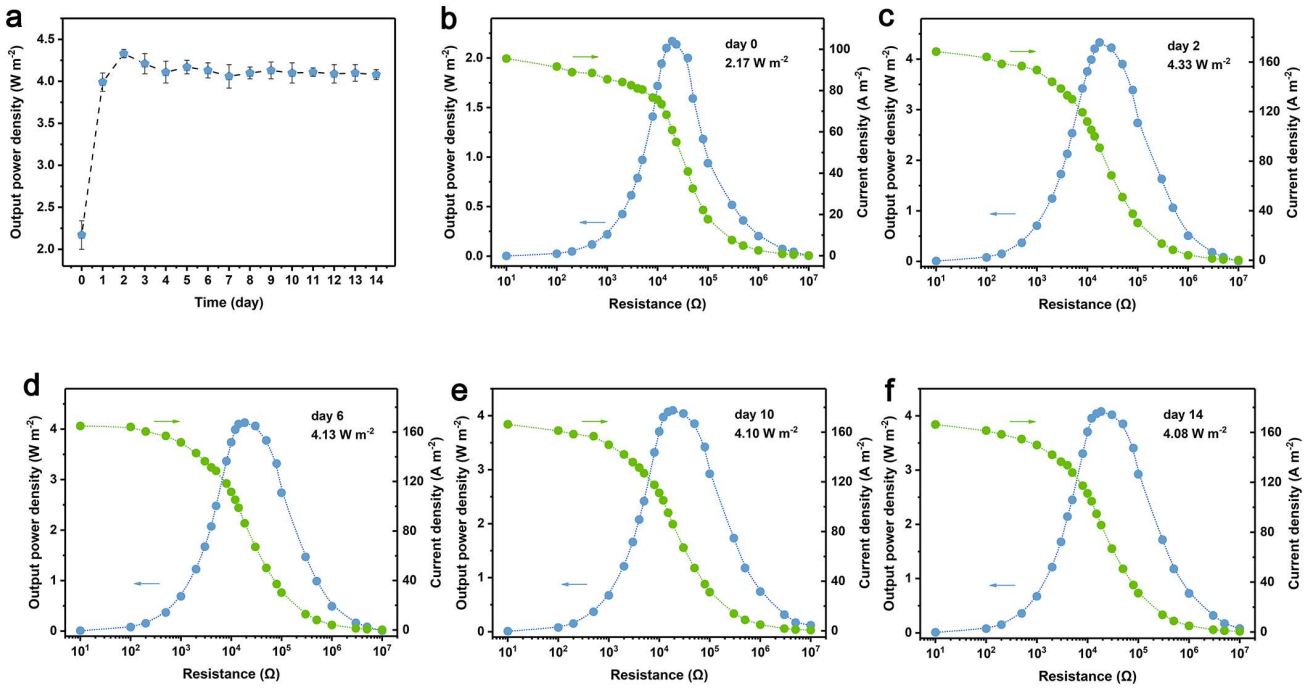

Figure S17. Long-term stability, current density and output power density of the Na-MTM/Exolit OP 550/STFA composite membrane for osmotic energy conversion in a 14-day test.

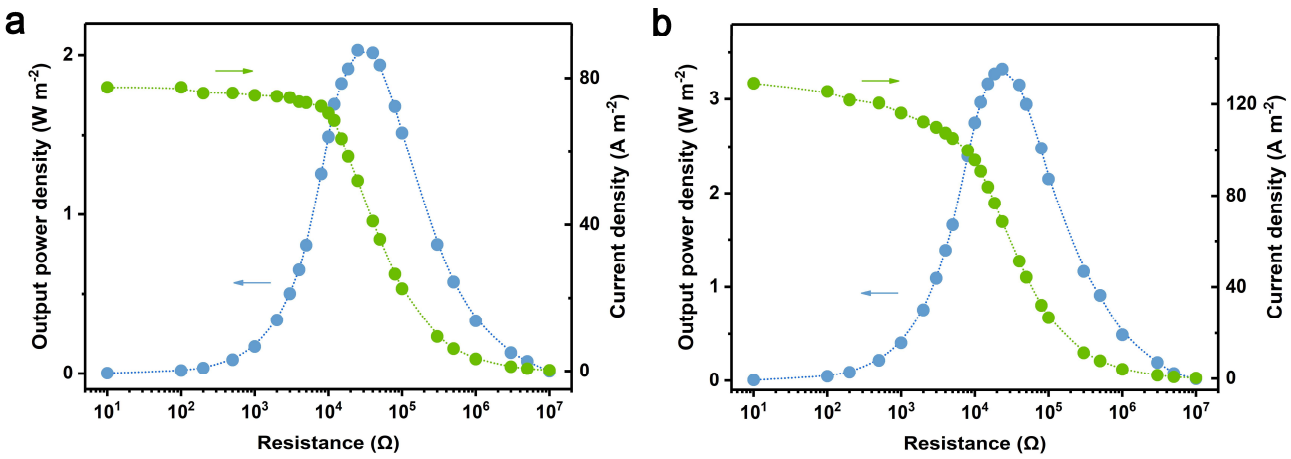

Figure S18. Current density and output power density of (a) Na-MTM/Exolit OP 550 and (b) Na-MTM/Exolit OP 550/SA composite membranes depend on the external load resistance in 0.5 M NaCl/0.01 M NaCl. The osmotic current density exhibits a rubbery plateau, followed by a continuous decrease with increasing R_L. The output power density calculated by the equation $P_L = I^2 \times R_L$ can be up to (a) 2.03 and (b) 3.32 W m^{-2} in 0.5 M NaCl/0.01 M NaCl when the R_L is comparable to the internal resistance of the membrane.

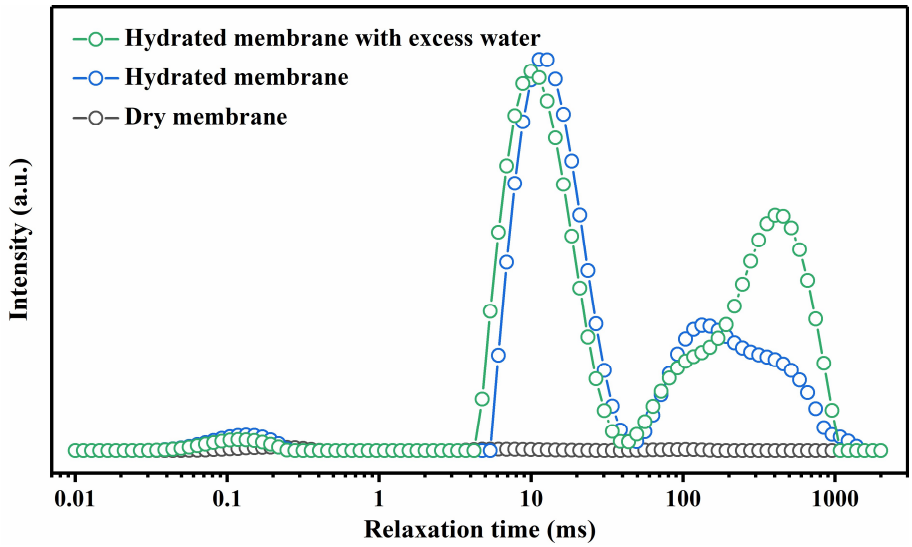

Figure S19. ^{1}H time-domain nuclear magnetic resonance spectra of SA modified Na-MTM composite membrane with ultrapure water as the probe molecule.

Table S1. The pH of Na-MTM powder suspension, Exolit OP 550 solution, and Na-MTM/Exolit OP 550 suspensions with different washing times.

	Exolit OP 550 solution	Na-MTM powder suspension	Na-MTM/Exolit OP 550 suspensions with different washing times				
			0	1	2	4	8
pH	2.20	8.04	1.87	3.06	3.84	4.32	4.89

Table S2. The corresponding values of V_{OC}, E_{redox}, V_{OS}, t_+, and η_{max}.

C_H/C_L (M/M)	$10^{-3}/10^{-4}$	$5.0\times10^{-3}/10^{-4}$	$10^{-2}/10^{-4}$	$2.5\times10^{-2}/10^{-4}$	$10^{-1}/10^{-4}$
E_{redox}	63	90	115	146	175
V_{OC}	110	154	191	236	279
V_{OS}	47	64	76	90	104
t_+	0.902	0.824	0.829	0.828	0.809
η_{max}	32.3	21.0	21.6	21.5	19.1

Table S3. Suspension ζ, surface ζ, and σ of the Na-MTM composite membranes.

Sample	Na-MTM/Exolit OP 550	Na-MTM/Exolit OP 550/SA	Na-MTM/Exolit OP 550/STFA
Suspension ζ (mV)	-33.8±0.2	-41.1±0.3	-35.5±0.2
Surface ζ (mV)	-37.7±0.4	-43.6±0.6	-42.1±0.3
σ (mC/m^2)	2.96±0.03	3.53±0.04	3.38±0.02

Table S4. Comparison of state-of-the-art two-dimensional nanofluidic membranes for osmotic energy harvesting. in 0.5 M NaCl/0.01 M NaCl.

Sample	Power density (W/m^2)	Testing area (mm^2)	Thickness (μm)	Internal resistance (kΩ)	Ref.
ANF/BN	0.40	3.14	1.0	10.0	3
PVMs	4.10	0.03	2.1	~13.0	4
SNF/GO	5.07	0.03	5.0	17.0	5
ANF/MTM	3.36	0.03	3.0	17.0	6
CNF/MoS_2	5.20	0.03	4.0	21.0	7
CNF/GO	4.19	0.03	9.0	24.0	8
BP/GO	2.50	0.03	8.0	25.0	9
ANF/GO	5.06	0.03	2.2	28.0	10
ANF/Mxene	3.70	0.03	4.5	29.0	2
BP/H_2O/O_2	1.60	0.03	8.0	-	9
BP/$(GO/BP)_3$	3.40	0.03	8.0	~30.0	9
Mxene	1.44	0.03	2.2	~35.0	2
GO	1.00	0.03	5.0	~50.0	5
MXene/BN	2.30	0.03	10.0	60.0	11
BP	0.50	0.03	8.0	220.0	9
MTM	3.68	0.03	15.2	-	12
Na-MTM/Exolit OP 550	**2.03**	**0.03**	**9.3**	**26.5**	**This work**
Na-MTM/Exolit OP 550/STFA	**4.10**	**0.03**	**9.3**	**19.2**	**This work**

Table S5. The material cost composition of 1 kg composite membranes.

Material	Composition	Price ($/kg)	Mass (g)	Total ($)	Ref.
BP	BP	179280000.0	1000.0	179280000.0	9
BP/GO or BP/(GO/BP)$_3$	BP	179280000.0	860.0	154180852.3	9
	Graphite powder	373.5	140.0		
CNF/MoS$_2$	MoS_2	597600.0	920.0	549887.6	7
	CNF	1195.0	80.0		
GO	Few-layer GO	119520.0	1000.0	119520.0	5
CNF/GO	Few-layer GO	119520.0	333.0	40597.2	8
	CNF	1195.0	667.0		
ANF/GO	Few-layer GO	119520.0	213.0	25847.5	10
	ANF	495.2	787.0		
SNF/GO	Few-layer GO	119520.0	213.0	25495.4	5
	SNF	47.8	787.0		
Mxene	Ti_3AlC_2	1080.0	1000.0	1080.0	2
ANF/Mxene	Ti_3AlC_2	1080.0	888.9	1015.0	2
	ANF	495.2	111.1		
MXene/BN	Ti_3AlC_2	1080.0	560.0	616.4	11
	h-BN	26.3	440.0		
MTM	MTM	565.6	1000.0	565.6	12
PVMs	PVMs	292.0	1000.0	292.0	4
ANF/MMT	MMT	128.5	888.9	169.2	6
	ANF	495.2	111.1		
Na-MTM/Exolit OP 550/STFA	Na-MTM	1.5	762.7	**76.2**	**This work**
	Exolit OP 550	12.9	84.7		
	STFA	485.3	152.5		

Table S6. Comparison of state-of-the-art organic framework membranes for osmotic energy harvesting.

Sample	Power density (W/m^2)	Testing area (mm^2)	Concentration gradient (M)	Internal resistance (kΩ)	Ref.
ZnTPP–COF	14.90	0.25	0.5: 0.01 NaCl	2.2	13
UiO-66-NH_2@ANM	2.96	0.03	0.5: 0.01 NaCl	~10.5	14
COF	5.90	0.03	0.5: 0.01 NaCl	19.4	15
MOF	7.00	0.03	0.5: 0.01 NaCl	~23.0	16
2DPI	65.20	$11.8*10^{-6}$	0.5: 0.01 NaCl	2000.0	17
COF@ANM	27.80	0.03	5: 0.01 NaCl	7.9	18
ZIF-8/PSS@ANM	23.40	0.03	2: 0 LiCl-methanol	11.5	19

References

1 Feng, J. *et al.* Single-layer MoS2 nanopores as nanopower generators. *Nature* **536**, 197-200, doi:10.1038/nature18593 (2016).

2 Zhang, Z. *et al.* Mechanically strong MXene/Kevlar nanofiber composite membranes as high-performance nanofluidic osmotic power generators. *Nature Communications* **10**, 2920, doi:10.1038/s41467-019-10885-8 (2019).

3 Chen, C. *et al.* Bio-inspired Nanocomposite Membranes for Osmotic Energy Harvesting. *Joule* **4**, 247-261, doi:https://doi.org/10.1016/j.joule.2019.11.010 (2020).

4 Cao, L. *et al.* Lamellar porous vermiculite membranes for boosting nanofluidic osmotic energy conversion. *Journal of Materials Chemistry A* **9**, 14576-14581, doi:10.1039/D1TA02400K (2021).

5 Xin, W. *et al.* Biomimetic Nacre-Like Silk-Crosslinked Membranes for Osmotic Energy Harvesting. *ACS Nano* **14**, 9701-9710, doi:10.1021/acsnano.0c01309 (2020).

6 Qin, R. *et al.* Nanofiber-reinforced clay-based 2D nanofluidics for highly efficient osmotic energy harvesting. *Nano Energy* **100**, 107526, doi:https://doi.org/10.1016/j.nanoen.2022.107526 (2022).

7 Zhu, C. *et al.* Metallic Two-Dimensional MoS2 Composites as High-Performance Osmotic Energy Conversion Membranes. *Journal of the American Chemical Society* **143**, 1932-1940, doi:10.1021/jacs.0c11251 (2021).

8 Wu, Y. *et al.* Enhanced ion transport by graphene oxide/cellulose nanofibers assembled membranes for high-performance osmotic energy harvesting. *Materials Horizons* **7**, 2702-2709, doi:10.1039/D0MH00979B (2020).

9 Zhang, Z. *et al.* Oxidation promoted osmotic energy conversion in black phosphorus membranes. *Proceedings of the National Academy of Sciences* **117**, 13959-13966, doi:doi:10.1073/pnas.2003898117 (2020).

10 Chen, J. *et al.* Biomimetic Nanocomposite Membranes with Ultrahigh Ion Selectivity for Osmotic Power Conversion. *ACS Cent Sci* **7**, 1486-1492, doi:10.1021/acscentsci.1c00633 (2021).

11 Yang, G. *et al.* Stable Ti3C2Tx MXene–Boron Nitride Membranes with Low Internal Resistance for Enhanced Salinity Gradient Energy Harvesting. *ACS Nano* **15**, 6594-6603, doi:10.1021/acsnano.0c09845 (2021).

12 Xiao, T. *et al.* Low-cost 2D nanochannels as biomimetic salinity- and heat-gradient power generators. *Nano Energy* **103**, 107782, doi:https://doi.org/10.1016/j.nanoen.2022.107782 (2022).

13 Yang, J. *et al.* Advancing osmotic power generation by covalent organic framework monolayer. *Nature Nanotechnology* **17**, 622-628, doi:10.1038/s41565-022-01110-7 (2022).

14 Liu, Y.-C., Yeh, L.-H., Zheng, M.-J. & Wu, K. C.-W. Highly selective and high-performance osmotic power generators in subnanochannel membranes enabled by metal-organic frameworks. *Science Advances* **7**, eabe9924, doi:doi:10.1126/sciadv.abe9924 (2021).

15 Hou, S. *et al.* Free-Standing Covalent Organic Framework Membrane for High-Efficiency Salinity Gradient Energy Conversion. *Angewandte Chemie International Edition* **60**, 9925-9930, doi:https://doi.org/10.1002/anie.202100205 (2021).

16 Zhao, X. *et al.* Metal organic framework enhanced SPEEK/SPSF heterogeneous membrane

for ion transport and energy conversion. *Nano Energy* **81**, 105657, doi:https://doi.org/10.1016/j.nanoen.2020.105657 (2021).

17 Zhang, Z. *et al.* Cation-selective two-dimensional polyimine membranes for high-performance osmotic energy conversion. *Nature Communications* **13**, 3935, doi:10.1038/s41467-022-31523-w (2022).

18 Gao, M. *et al.* A bioinspired ionic diode membrane based on sub-2 nm covalent organic framework channels for ultrahigh osmotic energy generation. *Nano Energy* **105**, 108007, doi:https://doi.org/10.1016/j.nanoen.2022.108007 (2023).

19 Fauziah, A. R., Chu, C.-W. & Yeh, L.-H. Engineered subnanochannel ionic diode membranes based on metal–organic frameworks for boosted lithium ion transport and osmotic energy conversion in organic solution. *Chemical Engineering Journal* **452**, 139244, doi:https://doi.org/10.1016/j.cej.2022.139244 (2023).